FOUNDRY WASTES AS A POTENTIAL PRECURSOR IN ALKALI ACTIVATION TECHNOLOGY

BARBARA HORVAT[1], ALENKA PAVLIN[2] &
VILMA DUCMAN[1]

[1] Slovenian National Building and Civil Engineering Institute, Department for Materials, Ljubljana, Slovenia, e-mail: barbara.horvat@zag.si, vilma.ducman@zag.si
[2] TERMIT, Moravče, Slovenia, e-mail: alenka.pavlin@termit.si

Abstract In this study the amount of amorphous phase of elements useful in alkali activation of waste materials produced by the foundry industry was determined. Waste foundry sands, foundry flue gas and waste casting cores were alkali activated, and waste green ceramics and bottom ash were added to one of the foundry sand samples to shorten the time for producing measurable compressive strength from 1.5 years to 1 week.

Keywords: alkali activated material, foundry wastes, compressive strength, upcycling, circular economy.

University of Maribor Press

DOI https://doi.org/10.18690/978-961-286-353-1.1
ISBN 978-961-286-353-1

1 Introduction

The ZAG national building institute and Termit, a mining company, started an upcycling project in 2017 in which different waste materials from several sources were used as precursors in alkali activation (AA) of potential lightweight insulating materials used in the building industry.

Alkali activated synthesis is the process of inorganic materials rich in amorphous Si and Al reacting with alkali (NaOH, KOH, Na-water glass, K-water glass) forming a semi-crystalline polymer structure of Si and Al connected with O bridges. Both Si and Al are in aluminosilicate network as SiO_4 and AlO_4 tetrahedrons that are joined by oxygen bridges. Compensation of the non-natural coordination number of Al is accomplished by amorphous cations from precursor or from an alkali solution (Provis, 2013, Provis and Bernal, 2014, Palomo *et al.*, 1999, Provis, 2014, van Deventer *et al.*, 2010, *Handbook of Alkali-Activated Cements, Mortars and Concretes*, 2015, Provis, 2018).

This technology offers savings to the building industry as a result of low processing costs due to the low temperature curing, and by using waste materials or byproducts instead of raw materials (Palomo and Fernández-Jiménez, 2011); at the same time, these materials have good physical properties and can be fire resistant (Hajimohammadi *et al.*, 2017).

The most thoroughly researched materials for alkali activation are fly-ash (Palomo *et al.*, 1999, Němeček *et al.*, 2011, Fernández-Jiménez and Palomo, 2005, Škvára *et al.*, 2009, Puertas and Ferna, 2003, Puertas *et al.*, 2000), slag (Puertas and Ferna, 2003, Shi and Qian, 2000, Puertas *et al.*, 2000, Pan *et al.*, 2002, Buchwald *et al.*, 2007, Bakharev *et al.*, 1999, Bernal *et al.*, 2012) and metakaolin (Pacheco-Torgal *et al.*, 2008, Němeček *et al.*, 2011, Buchwald *et al.*, 2007, Granizo *et al.*, 2004, Granizo *et al.*, 2000, Bernal *et al.*, 2012, Alonso and Palomo, 2001); however, there are many other waste materials produced by industry and by the demolition of buildings that could be used as precursors.

The focus of our work was to evaluate various foundry wastes upcycling with alkali activation technology into materials that can be used in the building industry. Termit collects these materials from foundries which use their casting cores and quartz sand in order to use these wastes for the rehabilitation of open pits.

Foundry fumes, flue gas and exhaust air (FFG) must be captured in the foundry industry ("European Commission Integrated Pollution Prevention and Control," 2005) because they present a health hazard (Tossavainen, 1976) to foundry workers (lung contamination (Kalliomäki *et al.*, 1979), respiratory disease (Ostiguy *et al.*, 1995, Low and Mitchell, 1985), and potential carcinogenicity (Humfrey *et al.*, 1996)); therefore, it is crucial to immobilize these gases, which can be done with alkali activation (Fernandez-Jimenez *et al.*, 2005b, Khalil and Merz, 1994, Nikolić *et al.*, 2014, Qian *et al.*, 2003, Fernandez-Jimenez *et al.*, 2005a, Guangren, 2002, Yunsheng *et al.*, 2007, Zhang *et al.*, 2008, Shi and Fernández-Jiménez, 2006, Deja, 2002).

Waste foundry sand (WFS) comprises in Termit the largest amount of all collected chemically inert and stable waste materials; therefore, it is logical to find other uses for it. Several studies in the civil engineering field have been conducted with WFS:

- In concrete production, where WFS replaced fine aggregate from 0 % to 100 %, and the water to cement ratio was constant. With increasing amounts of WFS, compressive strength decreased (from 43.6 MPa without WFS, to 32.9 MPa when 60 % WFS replaced fine aggregate, to almost half when only WFS was used – measured on 28th day), while shrinkage and water absorption increased (Khatib *et al.*, n.d.).
- In high-strength concrete production, fine natural sand was replaced with WFS in increments of 0 %, 5 %, 10 % and 15 %. Compressive strength increased with time but decreased with an increase in the ratio of WFS to natural sand. Optimal re-allocation happened at 10 % replacement of fine natural sand with WFS, where a decrease in compressive strength was from 61 MPa to 60 MPa (measured on 28th day). Concrete with more than 5 % WFS showed reduction in water absorption. The particle size distribution of WFS must be arranged to provide similar properties to concrete made with standard fine sand (Guney *et al.*, 2010).

- In ready-mixed concrete production, regular sand was replaced with 0 %, 10 %, 20 %, 30 % and 40 % WFS. Compressive strength and density decreased (from 43.2 MPa to 42.7 MPa when WFS replaced 10 % of the regular sand - measured on 28th day), while water absorption increased with the replacement of sand with WFS. 20 % WFS instead of regular sand does not compromise mechanical properties. Ni, Zn, Cr, F-, total dissolved solids, total organic carbon, and dissolved organic carbon were immobilized well at different pH conditions according to TS EN 12457-4:2004 (Basar and Deveci Aksoy, 2012).
- In concrete production, fine aggregates were partially replaced by bottom ash and WFS in equal amounts from 0 % to 60 %. Compressive strength after 28 days of up to 50 % replacement with WFS and bottom ash was from 29 MPa to 32 MPa (without replacement it was over 35 MPa), and after 1 year it was comparable to the compressive strength of concrete made with just fine aggregates, making 50 % substitution of fine aggregates the highest possible value. The highest compressive strength among all samples with WFS and bottom ash was demonstrated with a sample with 30 % replacement of fine aggregates (Aggarwal and Siddique, 2014).
- In low calcium fly ash alkali activated concrete and in ground granulated blast furnace slab based alkali activated concrete, WFS partially to entirely replaced normal sand, in proportions of 0 %, 20 %, 40 %, 60 %, 80 % and 100 %. A mixture of sand and WFS was added to a mixture of slag/ash and ordinary Portland cement. Whole dry content was alkali activated with 14 M NaOH, Na-water glass and tap water, where the ratio was NaOH(aq):Na-water glass=1:2.3; the mass % (m%) of aggregates to the whole was 76 %, and the m% of alkaline solution was 45 % of powdered binder. The mixture was cured in moulds for 24 h, and compressive strength measured at 28 days, when the alkali activated slag concrete showed higher strength than alkali activated fly ash concrete, no matter the amount of WFS. The highest compressive strength with fly ash concrete was with 60 % of WFS (48.5 MPa), while the highest compressive strength with slag concrete was with 20 % of WFS (above 55 MPa from Fig. 5, Bhardwaj and Kumar, 2019).
- In alkali activation, WFS was used as a precursor and activated with NaOH/KOH of different molarity (6, 8, 10, 12, 14 M), and/or Na-water glass with/without addition of water, cured at room temperature and at 70 °C for 24 h, dried at room temperature and at 110 °C for 24 h, or in a

microwave for 2.3 min. The highest compressive strength was 27.7 MPa gained with only Na-glass water. The addition of water ruined the compressive strength, while drying at elevated temperature or with microwaves increased its value, but at the same time, it severely decreased bending strength (Horvat *et al.*, 2019).

2 Experimental

For research on a laboratory scale, waste casting cores, waste foundry sands, foundry flue gas, a mixture of bottom and fly ash, and waste green ceramics, presented in Table 1 (with sample label and waste label from the Classification list of waste from Official Gazette of the Republic of Slovenia, no. 20/01 Annex 1) were collected from Termit's open waste dumps. The last two waste materials listed were used only as a supplement to foundry sand.

Table 1: Analysed Termit's samples collected from waste dump piles.

Sample	Sample label	Waste label
Waste casting cores	WCC	10 09 06
Waste foundry sand A	WFS-A	10 09 08
Waste foundry sand B	WFS-B	10 09 08
Waste foundry sand C	WFS-C	10 09 08
Foundry flue gas	FFG	10 09 10
Mixture of bottom and fly ash	ASH	10 01 01
Waste green ceramics	WGC	10 12 01

Source of labels: Official Gazette of the Republic of Slovenia, no. 20/01 Annex 1

Chemical (X-ray fluorescence; XRF) and mineralogical (X-ray powder diffraction; XRD) analyses were performed on all samples, which were dried to remove H2O with an IR dryer at 105 °C to constant mass, and were afterwards ground in a vibrating disk mill (Siebtechnik) and sieved below 90 μm.

XRD analysis was performed (Empyrean PANalytical X-Ray Diffractometer, Cu X-Ray source) in steps of 0.0263° from 4° to 70°, under cleanroom conditions, in powder sample holders with an aperture diameter of 27 mm. Mineral analysis, with Rietveld refinement using external standard (pure Al2O3 crystal) to determine the

amount of amorphous phase and minerals, was performed with X'Pert Highscore plus 4.1 on XRD data.
Loss of ignition (LOI) was performed on dried powder samples at 950 °C for 2 h in a furnace (Nabertherm B 150) to remove organic compounds and CO2. LOI was determined with the gravimetric method from 2 parallel measurements and corrected with XRF analytical LOI obtained on a fused basis.

For XRF analysis (Thermo Scientific ARL Perform'X Sequential XRF), ignited material was mixed with Fluxana (FX-X50-2, Lithium tetraborate 50 % / Lithium metaborate 50 %) in a ratio of 1:10 for Fluxana to lower the melting temperature in a Claisse furnace from The Bee Electric Fusion (to avoid gluing of melt in the platinum vessel, a few drops of LiBr were added to the Fluxana powder mixture). Analysis of the melted disks was performed with OXAS software, and the data were analyzed with UniQuant 5 software.

A scanning electron microscopy (SEM; Jeol JSM-IT500 with tungsten filament cathode) investigation was performed under high vacuum conditions on dried samples.

For alkali activation, samples were dried at 70 °C for 24 h in a WTB Binder dryer without any further treatment if not stated otherwise. 10 M NaOH (Donau Chemie Ätznatron Schuppen, EINECS 215-785-5) and Na-water glass (Geosil, 344/7, Woelner) were mixed in a mass ratio of 1:1, stirred until the liquid became clear, and poured into the sample under constant mixing. The amount of precursor to liquid phase, presented in Table 2, was determined experimentally with a viscometer (Haake PK 100, VT 500, PK2 1.0°), where the limit was the point where viscosity could not be measured any longer due to overload of torque (the WCC sample was ground below 2 different sizes of particles, while samples with smaller particles needed more liquid phase because of enlarged surface area).

Table 2: Mass percent ratio of precursor, 10 M NaOH and Na-water glass.

$m_{\%}$ ratio Sample label	Precursor	10 M NaOH	Na-water glass
WCC[a]	2.5	1	1
WCC[b]	3.3	1	1
WFS-A	4	1	1
WFS-B	3	1	1
WFS-C	3	1	1
FFG	5	1	1
ASH	3	1	1

a - ground below < 90 μm; b - gently ground below < 600 μm

The WFS-C sample was mixed with ASH in a mass ratio of 1:1, and with ASH and WGC in a ratio of 1:1:1. The mass ratio of mixed dry precursor to 10 M NaOH and Na-water glass was 3:1:1.

Samples were moulded into prisms of 80x20x20 mm3 (sample WCC ground and sieved below 90 μm into prisms of 25x12x12 mm3) and cured at 70 °C for 24 h, or at room temperature. After demolding, they were left to dehydrate and solidify at room conditions for as long as needed, if not stated otherwise (see section 3.2). The compressive strength of alkali activated samples was measured with a compressive and bending strength testing machine (ToniTechnik ToniNORM), and samples were measured by means of SEM (under high vacuum conditions).

3 Results and discussion

Ignition losses at 950 °C of all samples are presented in Table 3.

Table 3: LOI determined with gravimetric method and calculated from XRF data.

Laboratory sample label	LOI (950 °C) [%]	LOI (XRF) [%]
WCC	2.5	3.4
WFS-A	5.2	6.5
WFS-B	6.8	7.6
WFS-C	4.0	6.3
FFG	12.7	14.6
ASH	17.7	18.9
WGC	6.5	7.4

The ignition loss of ASH was highest among tested samples (18.9 %) as a result of incomplete combustion in the process. Foundry flue gas has lower LOI (14.6 %), also due to incomplete combustion (from XRF analysis, see Table 4, there is not much CaO and MgO for potential carbonization, which could be the reason for the higher LOI).

All 3 WFS (A, B, C) and WGC have comparable LOI (around 6-7 %), while WCC has the lowest LOI (3 %) because of the high percentage of quartz in the sample (95.7 %, see Table 5).

3.1 Chemical and mineralogical analysis

The amount of different oxides was measured with XRF analysis. The results where the mass percentage of oxides is close to or above 0.1 % are presented in Table 4.

Table 4: Mass percentage ($m_{\%}$ [%]) of oxides measured with XRF.

Sample label	Na_2O	MgO	Al_2O_3	SiO_2	P_2O_5	SO_3	K_2O
WCC			2.5	95.6			0.1
WFS A	0.6	0.6	3.9	90.7			0.3
WFS B	0.2	0.3	3.6	87.7			0.2
WFS C	1.5		0.6	94.0			0.1
FFG	0.7	0.7	8.4	83.5			0.2
ASH	0.3	9.4	10.5	26.9	1.0	2.7	4.1
WGC	0.3	1.4	23.1	61.6			4.4

Table 4: Cont'd.

Sample label	CaO	TiO_2	Cr_2O_3	MnO	Fe_2O_3	ZnO	SrO	BaO
WCC	0.1	0.08			0.5			
WFS A	0.9	0.2			1.2			
WFS B	0.5	1.0		0.3	5.0	0.08		
WFS C	0.2	0.08			0.8			
FFG	1.4	0.6			2.2			
ASH	25.3	0.6		0.4	16.8		0.09	0.2
WGC	3.4	0.2	0.8	1.5	1.5			0.4

In all samples, SiO_2 was among the most commonly detected oxides, even in bottom ash, which also had high amounts of CaO, Fe_2O_3, MgO and Al_2O_3. The latter was also present in all samples, where the highest amount, double that compared to ASH, was found in WGC. Other oxides were detected in the samples in quantities of less than 5 %.

Minerals in all precursors determined with Rietveld refinement from XRD are presented in Fig. 1, with the goodness of fit (GOF) below 8.8. All foundry waste materials contain only quartz (from 62 to 96 mass percent); the rest is in the amorphous phase. ASH, on the other hand, contains katoite, quartz, calcite, magnetite and brownmillerite (from highest to lowest amounts), while GWC contains quartz, corundum, ankerite, calcite and magnesioferrite brownmillerite (from highest to lowest amounts).

Elements in precursors (and both mixtures) useful for alkali activation, i.e. elements that are in the amorphous phase, calculated as the difference in mass % between the XRF and XRD results (all elements present in the samples minus all elements in crystalline form), are presented in Table 5. The least promising precursor (containing low amounts of Si and Al) is WCC; among the most promising WFS samples are WFS-B and WFS-C, and the least promising is WFS-A. FFG is more promising for alkali activation compared to ASH, while the most promising material among all of the samples is WGC.

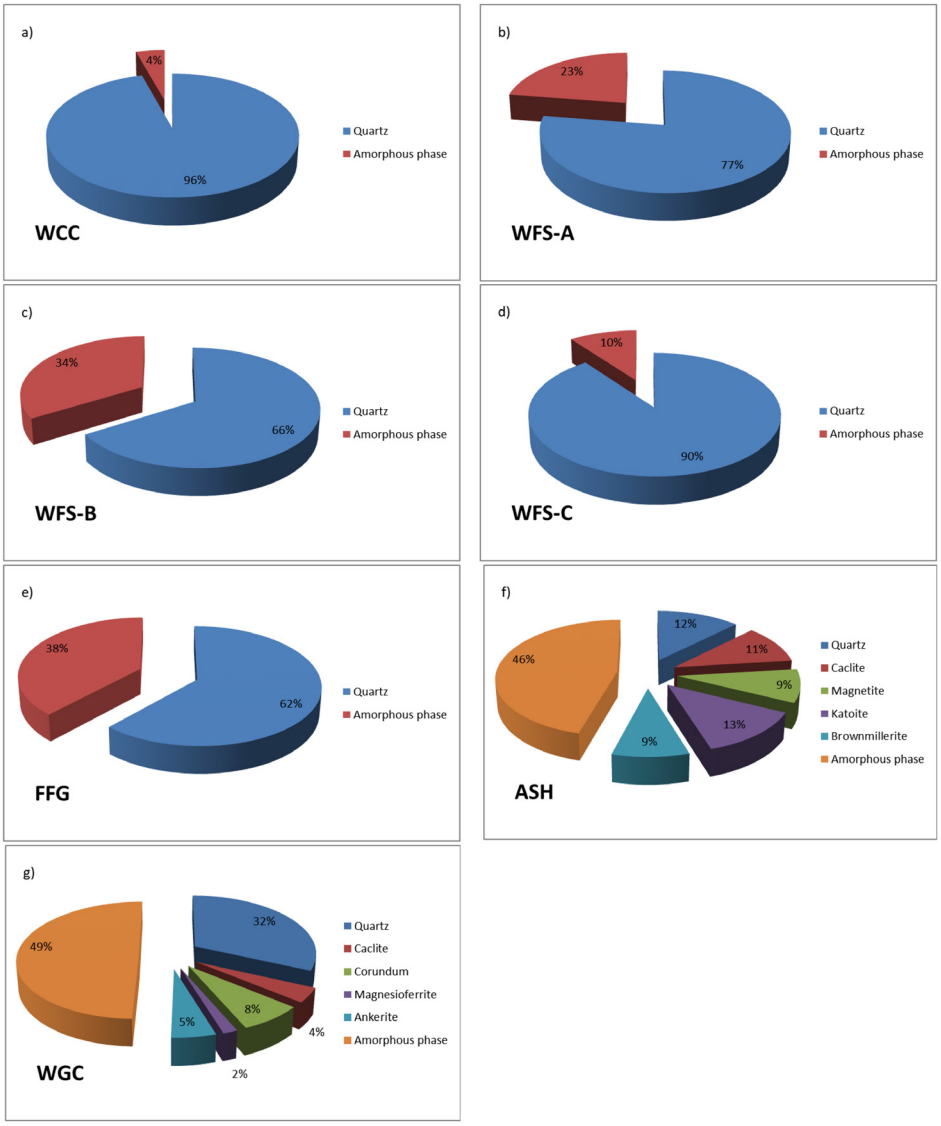

Figure 1: Rietveld refinement of XRD results for a) WCC; WFS b) A. c) B, and d) C; e) FFG; f) ASH; g) WGC.

Table 5: Mass percent ($m_{\%}$ [%]) of amorphous elements useful in alkali activation.

Element [$m_{\%}$]	Na	K	Mg	Ca	Sr	Ba	Al	Si
WCC	0	0.1	0	0.1	0	0	1.3	0.02
WFS A	0.5	0.3	0.4	0.6	0	0.04	2.0	6.2
WFS B	0.2	0.2	0.2	0.3	0	0.02	1.9	10.1
WFS C	1.1	0.1	0.03	0.1	1	1.04	0.3	2.0
FFG	0.5	0.2	0.4	1.0	0.01	0.04	4.4	10.2
ASH	0.2	3.4	5.7	6.9	0.1	0.2	3.5	6.7
WGC	0.3	3.7	0.2	0	0.02	0.4	8.2	14.0
WFS-C+ASH	0.6	1.8	2.8	3.5	0.04	0.1	1.9	4.4
WFS-C+ASH+WGC	0.5	2.4	1.9	2.2	0.03	0.2	4.0	7.6

3.2 Mechanical analysis

Compressive strength, one of the most important properties in the building industry, is presented in Table 6, with density, time of solidification and measurement. All three WFS tested exhibited slow reactions, where only WFS-A solidified in a few days (compressive strength was 11 MPa measured after 3 months), while the other two (WFS-B and WFS-C) needed approximately 1.5 years at room conditions (compressive strength after 3 months could not be measured). Addition of ASH to WFS-C reduced the solidification time to 1 week (compressive strength was 3 MPa measured after 3 months), while the addition of GWC to WFS-C and ASH further increased compressive strength to 8 MPa, measured after 3 months. FFG solidified in a day with compressive strength of 10 MPa measured after 3 months. WCC, on the other hand, did not show promising results under mild conditions described in the following section.

Table 6: Mechanical properties of alkali activated material prepared from foundry wastes, bottom ash and waste green ceramics.

Sample label	Time of solidification	Time between moulding and measurement	Density [kg/l]	Compressive strength [MPa]
WCC < 90 μm	**Did not solidify in more than 2 years (stayed rubber-like)**			
WCC < 600 μm			**Fell apart at demolding**	
WFS-A	< 1 week	3 months	1.6	10.7
WFS-B	~ 1.5 year	~ 1.5 year	1.5	6.1
WFS-C	~ 1.5 year	~ 1.5 year	1.6	12.9
FFG	< 1 week	3 months	1.5	10.5
ASH	< 1 week	3 months	1.3	5.2
WGC	< 1 week	3 months	1.5	25.8
WFS-C+ASH	< 1 week	3 months	1.5	3.2
WFS-C+ASH +WGC	< 1 week	3 months	1.5	8.0

3.3 Microstructural analysis

A SEM micrograph (left magnified 50 times, middle magnified ~500 times) of WCC, original and ground, is presented in Fig. 2 (a1 and a2 respectively). In the same Fig., WFS-A (b) and WFS-B (c) are shown. Fig. 3 shows WFS-C (d), FFG (e), ASH (f) and WGC (g). The photos on the right in Fig. 2 and Fig. 3 are photos of the collected samples and samples prepared for AA.

Although there is no significant difference between all 3 WFS under 50 times magnification, there is a difference in the surface when the unground precursors are magnified 500 times; WFS-A has the smoothest surface, WFS-B is slightly rougher, while WFS-C consists mostly of plates and needles.

WCC, gently ground in a mortar with pestle and sieved below 600 μm, and "WFS" before being used in the foundry industry, gently ground in a mortar with pestle and sieved below 1 mm, are comparable under 50 times magnification to all 3 WFS, from which WFC-B and WFS-C were gently ground in a mortar with pestle and sieved below 1 mm, while under 500 times magnification, the surface of WCC is much smoother. Darker particles of sand have more organic compounds on the surface, which are used to "glue" sand into casting cores. In the sample there were also radiolarians, one marked with a red square in Fig. 2 (a1).

WCC ground in a vibrating disk mill (Siebtechnik) and sieved below 90 μm consisted of mostly "plate-like" rocks with sharp edges.

A mixture of bottom and fly ash (most of it bottom ash) consisted of typical spherical particles (like those found in fly ash), cenospheres (red square in Fig. 3 (f)), mineral aggregates (quartz), (Kutchko and Kim, 2006), and a number of needles aggregated or grown into hedgehog-like structures not found in fly-ash.

GWC consists of plate-like structures with sharp edges, probably ground before further processes in the ceramic industry.

Bottom ash and GWC were gently ground in a mortar with a pestle and sieved below 1 mm for AA.
The SEM of alkali activated materials is presented in Fig. 4, Fig. 5 and Fig. 6; the first two were made from "pure" waste materials, and the latter was made from mixtures of waste materials.

AA of WCC was not successful when the precursor used was ground below 600 μm; the prism fell apart upon demolding and could not support its own weight (see Fig. 4 a1); when the material was ground below 90 μm, the sample foamed, and could be successfully demoulded, but only if the mould used was smaller; however, the material did not solidify in 2 years (it stayed rubber-like). The experiment can not be scaled up under the mild experimental conditions used in this study. For high vacuum SEM, the sample was dried in a vacuum (Fig. 4 a2).

Alkali activated materials from all 3 WFS foamed and looked similar (i.e. sand stones covered with matrix) under low magnification (Fig. 4 b, c left and Fig. 5 d), but there are differences in the matrix itself which are obvious under higher magnification (Fig. 4 b, c and d right).

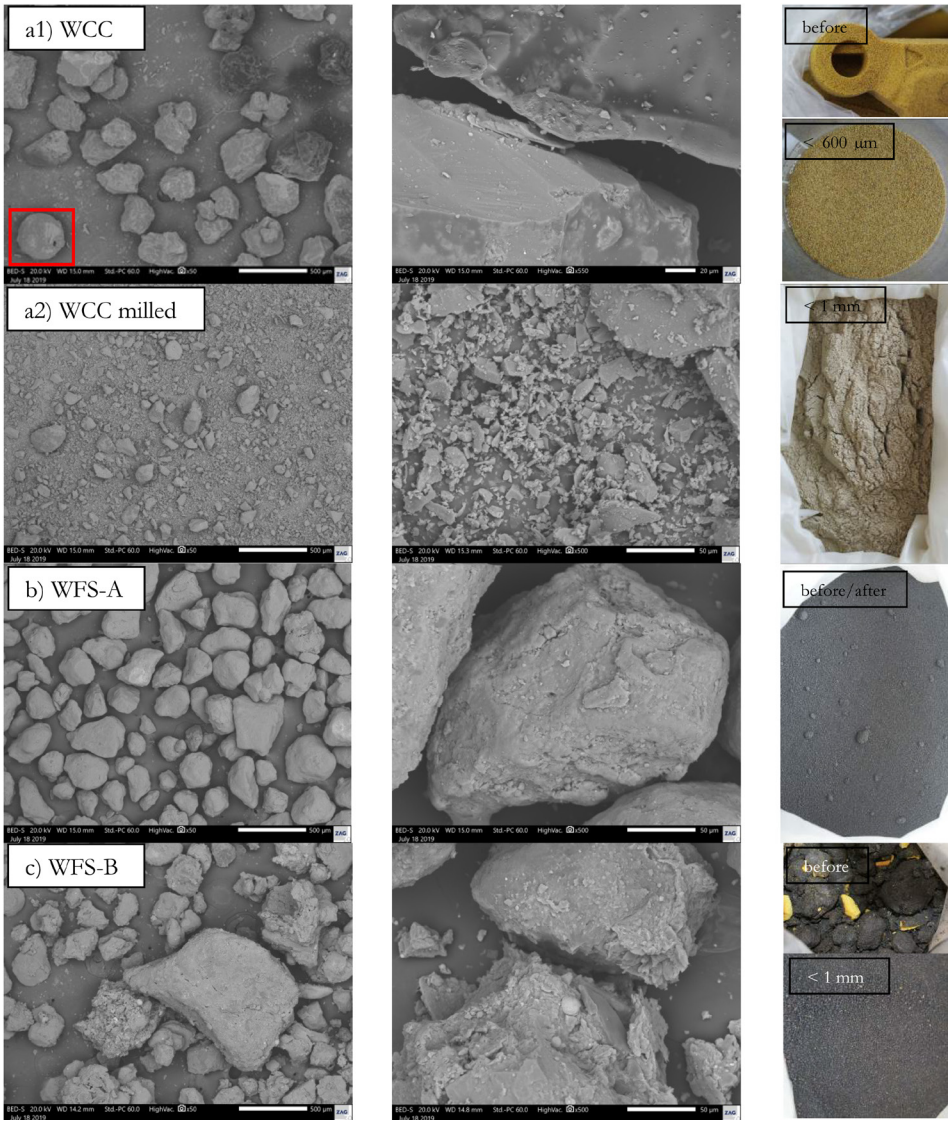

Figure 2: SEM micrographs of precursors magnified 50 and ~500-times with a photo of precursor before and after preparation for AA: a1) WCC gently ground and sieved below 600 µm (radiolaria is marked with a red square); a2) WCC milled and sieved below 90 µm; WFS from b) WFS-A, and c) WFS-B.

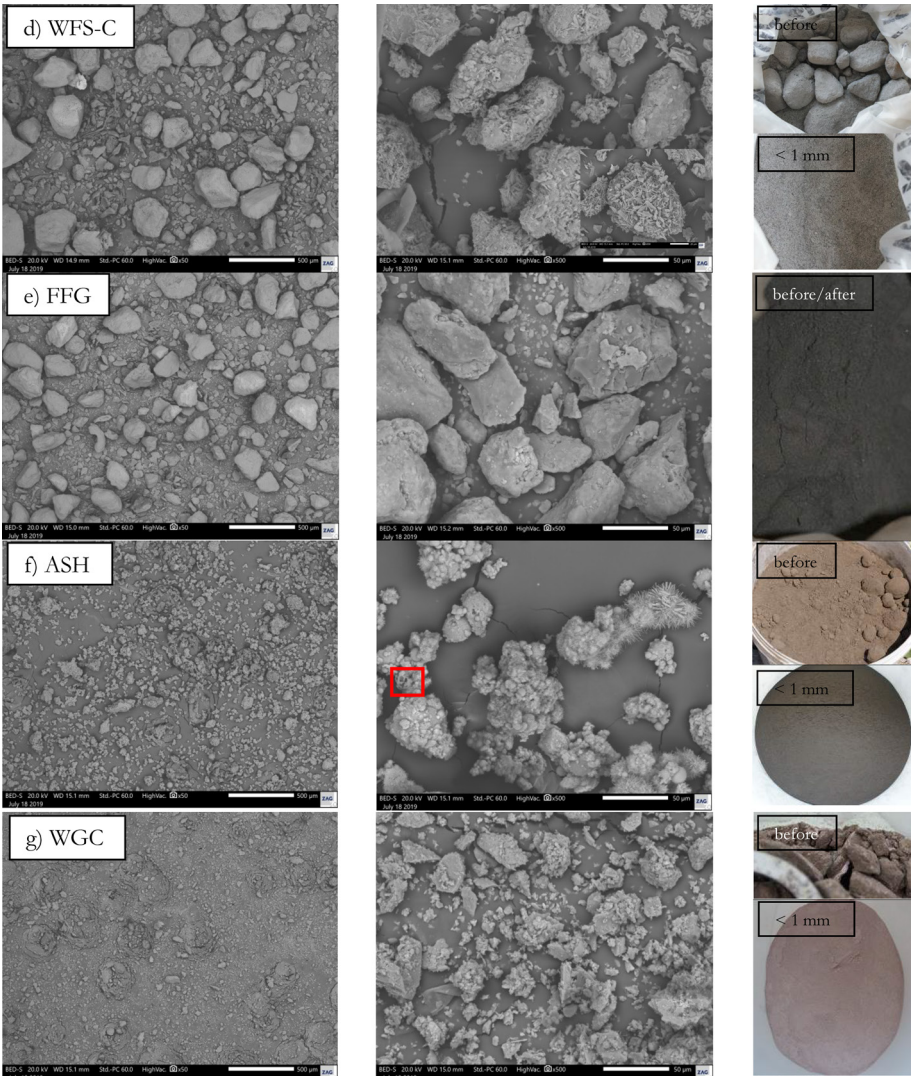

Figure 3: SEM micrographs of precursors magnified 50 and 500 times with photo of precursor before and after preparation for AA: d) WFS-C (inset: enlarged agglomerate of plates and needles); e) FFG; f) ASH (inset: mineral aggregate, quartz; red square: cenosphere); g) WGC.

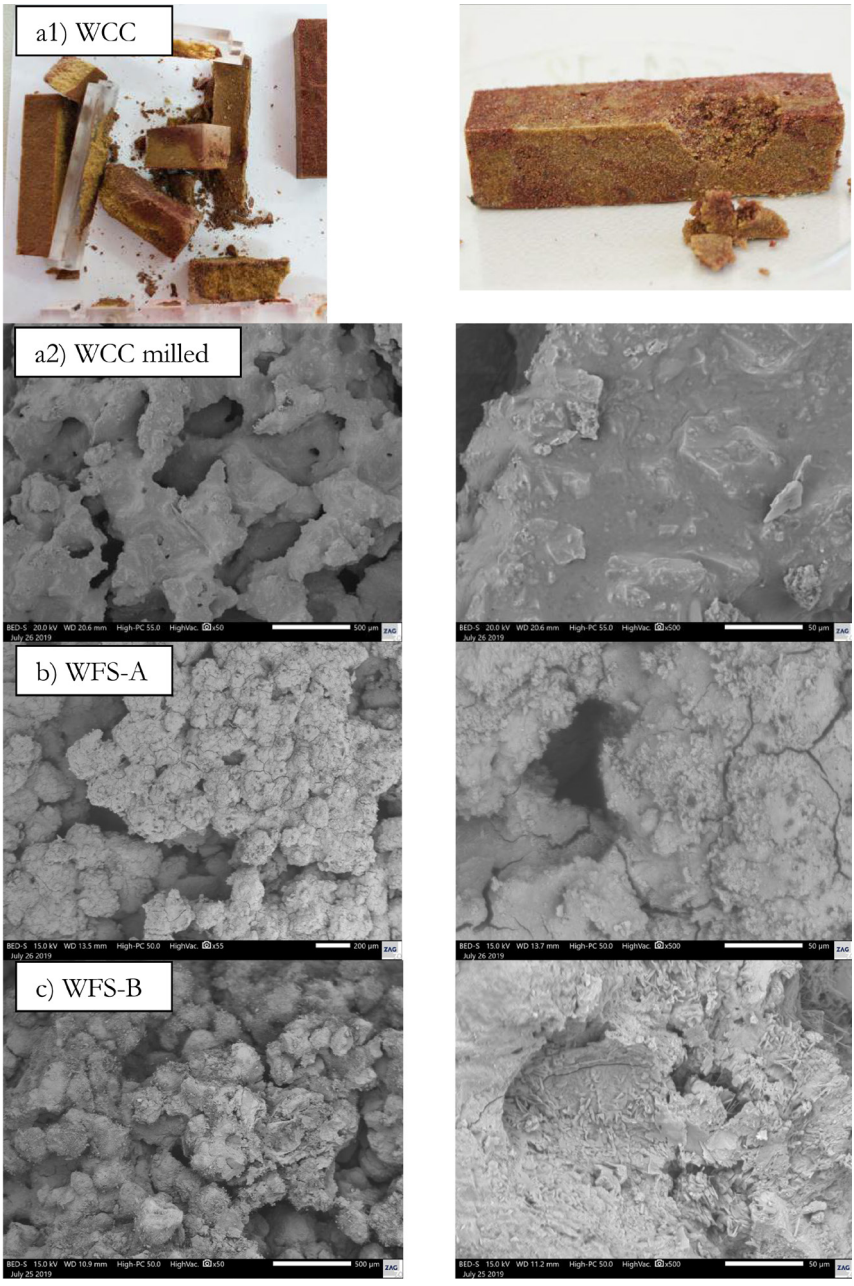

Figure 4: Photo/SEM micrographs, magnified 50 and 500 times, of alkali activated materials made using: a1) WCC gently ground and sieved below 600 μm; a2) WCC milled and sieved below 90 μm; b) WFS-A, and c) WFS-B.

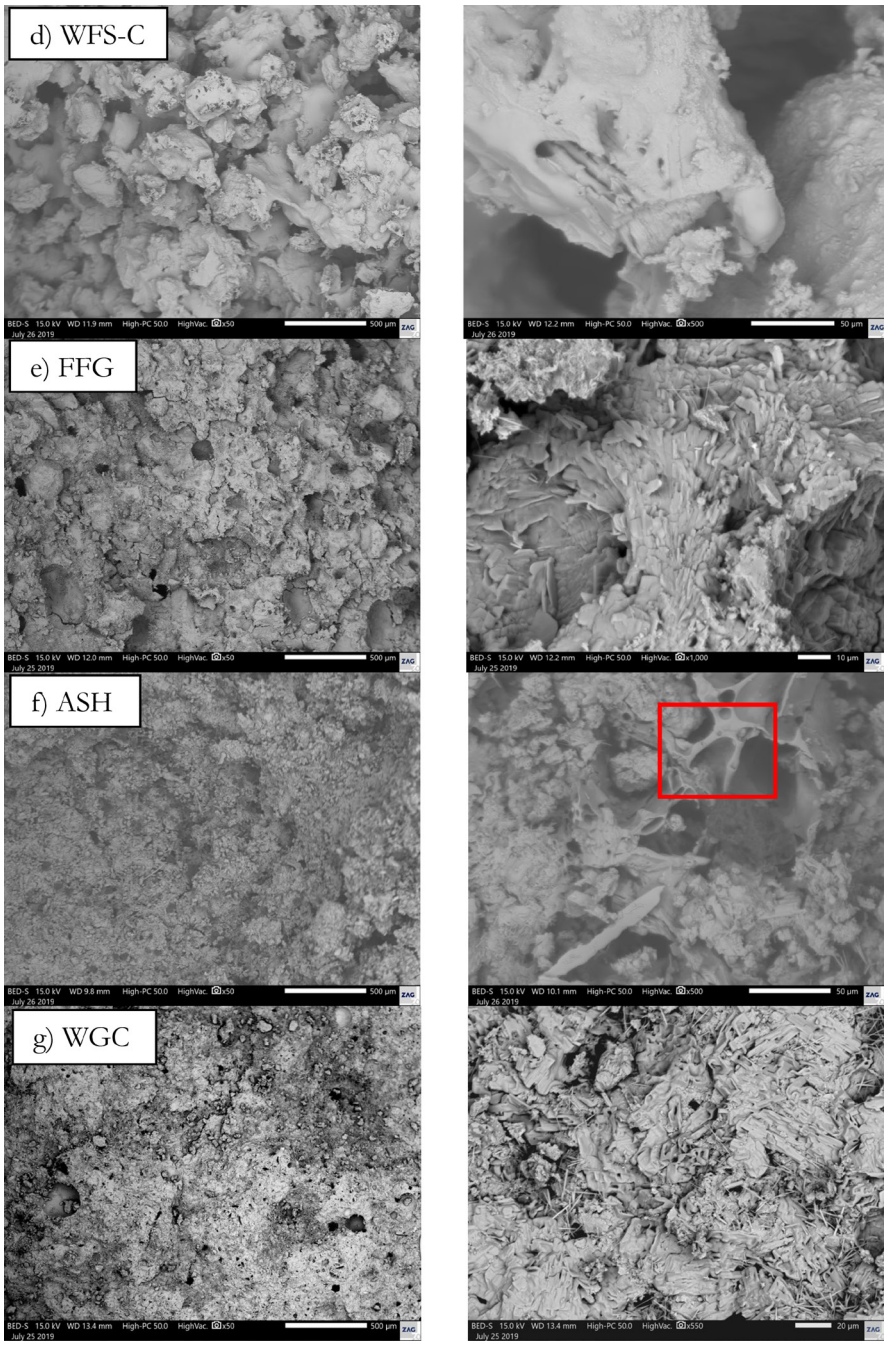

Figure 5: SEM micrographs magnified 50 and 500 times of alkali activated materials made using: d) WFS-C; e) FFG; f) ASH; g) WGC.

Alkali activated materials from FFG, bottom ash and WGC also appeared to be comparable under low magnification (Fig. 5 e, f and g left), while the matrix itself was similar only for alkali activated materials prepared from FFG and WGC (Fig. 5 e, f and g right), while material from FFG looked huskier, and material from WGC contained a large number of needles (efflorescence of salt). In alkali activated material from bottom ash, cellulose marked with a red square in Fig. 5 f (right) remained from the incomplete combustion of coal, making these materials the least waterproof among all 3 similar samples; it starts to decay in water immediately.

Since alkali activated materials from bottom ash and WGC solidify in a very short time, these precursors were used for the least promising precursor among WFS, WFS-C, according to the amount of amorphous elements needed in alkali activation. The addition of bottom ash to WFS-C, as shown in Fig. 5 h, shortened solidification by more than 5 times, and changed the look of the alkali activated material, while the matrix of the mixture was unique. Addition of WGC to the mixture, shown in Fig. 5 i, shortened the solidification time even more, and left the look of the matrix comparable to that of bottom ash, while the matrix itself changed completely (in the inset SEM micrograph there is cenosphere present from the bottom ash).

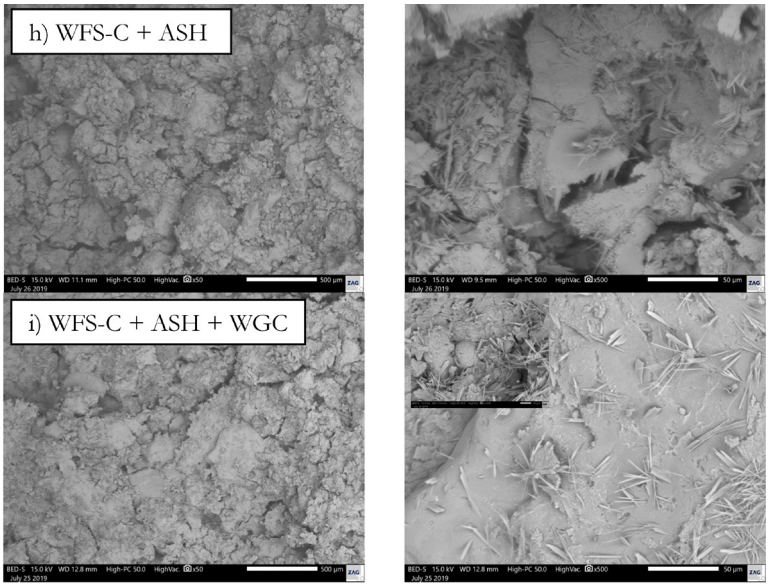

Figure 6: SEM micrographs of alkali activated materials made using a mixture of WFS-C and h) ASH; and i) ASH and WGC.

4 Conclusion

Alkali activation of foundry waste has potential in alkali activation as an aggregate, or as a precursor, or even as a potential foaming agent that is an aggregate at the same time. We have shown that with careful selection of precursors, we can control the time of solidification and matrix design, and obtain acceptable compressive strengths.

Acknowledgements

Project No. C3330-17-529032 "Raziskovalci-2.0-ZAG-529032" was granted by the Ministry of Education, Science and Sport of the Republic of Slovenia. The investment is co-financed by the Republic of Slovenia, Ministry of Education, Science and Sport and the European Regional Development Fund.

The Metrology Institute of the Republic of Slovenia is acknowledged for the use of XRF.

References

Aggarwal, Y., Siddique, R., 2014. Microstructure and properties of concrete using bottom ash and waste foundry sand as partial replacement of fine aggregates. Constr. Build. Mater. 54, 210–223. https://doi.org/10.1016/j.conbuildmat.2013.12.051

Alonso, S., Palomo, A., 2001. Alkaline activation of metakaolin and calcium hydroxide mixtures: influence of temperature, activator concentration and solids ratio. Mater. Lett. 47, 55–62. https://doi.org/10.1016/S0167-577X(00)00212-3

Bakharev, T., Sanjayan, J.G., Cheng, Y.-B., 1999. Alkali activation of Australian slag cements. Cem. Concr. Res. 29, 113–120. https://doi.org/10.1016/S0008-8846(98)00170-7

Basar, H.M., Deveci Aksoy, N., 2012. The effect of waste foundry sand (WFS) as partial replacement of sand on the mechanical, leaching and micro-structural characteristics of ready-mixed concrete. Constr. Build. Mater. 35, 508–515. https://doi.org/10.1016/j.conbuildmat.2012.04.078

Bernal, S.A., Mejía de Gutiérrez, R., Provis, J.L., 2012. Engineering and durability properties of concretes based on alkali-activated granulated blast furnace slag/metakaolin blends. Constr. Build. Mater. 33, 99–108. https://doi.org/10.1016/j.conbuildmat.2012.01.017

Bhardwaj, B., Kumar, P., 2019. Comparative study of geopolymer and alkali activated slag concrete comprising waste foundry sand. Constr. Build. Mater. 209, 555–565. https://doi.org/10.1016/j.conbuildmat.2019.03.107

Buchwald, A., Hilbig, H., Kaps, Ch., 2007. Alkali-activated metakaolin-slag blends—performance and structure in dependence of their composition. J. Mater. Sci. 42, 3024–3032. https://doi.org/10.1007/s10853-006-0525-6

Deja, J., 2002. Immobilization of Cr6+, Cd2+, Zn2+ and Pb2+ in alkali-activated slag binders. Cem. Concr. Res. 32, 1971–1979. https://doi.org/10.1016/S0008-8846(02)00904-3

European Commission Integrated Pollution Prevention and Control [WWW Document], n.d. URL http://eippcb.jrc.ec.europa.eu/reference/BREF/sf_bref_0505.pdf (accessed 7.17.19).

Fernandez-Jimenez, A., Macphee, D.E., Lachowski, E.E., Palomo, A., 2005a. Immobilization of cesium in alkaline activated fly ash matrix. J. Nucl. Mater. 346, 185–193. https://doi.org/10.1016/j.jnucmat.2005.06.006

Fernández-Jiménez, A., Palomo, A., 2005. Composition and microstructure of alkali activated fly ash binder: Effect of the activator. Cem. Concr. Res. 35, 1984–1992. https://doi.org/10.1016/j.cemconres.2005.03.003

Fernandez-Jimenez, A., Palomo, A., Macphee, D.E., Lachowski, E.E., 2005b. Fixing Arsenic in Alkali-Activated Cementitious Matrices. J. Am. Ceram. Soc. 88, 1122–1126. https://doi.org/10.1111/j.1551-2916.2005.00224.x

Granizo, M.L., Alonso, S., Blanco-Varela, M.T., Palomo, A., 2004. Alkaline Activation of Metakaolin: Effect of Calcium Hydroxide in the Products of Reaction. J. Am. Ceram. Soc. 85, 225–231. https://doi.org/10.1111/j.1151-2916.2002.tb00070.x

Granizo, M.L., Blanco-Varela, M.T., Palomo, A., 2000. Influence of the starting kaolin on alkali-activated materials based on metakaolin. Study of the reaction parameters by isothermal conduction calorimetry 7.

Guangren, Q., 2002. Improvement of metakaolin on radioactive Sr and Cs immobilization of alkali-activated slag matrix. J. Hazard. Mater. 92, 289–300. https://doi.org/10.1016/S0304-3894(02)00022-5

Guney, Y., Sari, Y.D., Yalcin, M., Tuncan, A., Donmez, S., 2010. Re-usage of waste foundry sand in high-strength concrete. Waste Manag. 30, 1705–1713. https://doi.org/10.1016/j.wasman.2010.02.018

Hajimohammadi, A., Ngo, T., Mendis, P., Kashani, A., van Deventer, J.S.J., 2017. Alkali activated slag foams: The effect of the alkali reaction on foam characteristics. J. Clean. Prod. 147, 330–339. https://doi.org/10.1016/j.jclepro.2017.01.134

Handbook of Alkali-Activated Cements, Mortars and Concretes, 2015. . Elsevier. https://doi.org/10.1016/C2013-0-16511-7

Horvat, B., Ducman, V., Pavlin, A.S., 2019. Waste Foundry Sand as Precursor in Alkali Activation Process. Livar. Vestn. 66, 13.

Humfrey, C.D.N., Levy, L.S., Faux, S.P., 1996. Potential carcinogenicity of foundry fumes: a comparative in vivo-in vitro study. Food Chem. Toxicol. 34, 1103–1111. https://doi.org/10.1016/S0278-6915(97)00081-1

Kalliomäki, P.-L., Korhonen, O., Mattsson, T., Sortti, V., Vaaranen, V., Kalliomäki, K., Koponen, M., 1979. Lung contamination among foundry workers. Int. Arch. Occup. Environ. Health 43, 85–91. https://doi.org/10.1007/BF00378146

Khalil, M.Y., Merz, E., 1994. Immobilization of intermediate-level wastes in geopolymers. J. Nucl. Mater. 211, 141–148. https://doi.org/10.1016/0022-3115(94)90364-6

Khatib, J.M., Baig, S., Bougara, A., Booth, C., n.d. Foundry Sand Utilisation in Concrete Production 8.

Kutchko, B., Kim, A., 2006. Fly ash characterization by SEM–EDS. Fuel 85, 2537–2544. https://doi.org/10.1016/j.fuel.2006.05.016

Low, I., Mitchell, C., 1985. Respiratory disease in foundry workers. Occup. Environ. Med. 42, 101–105. https://doi.org/10.1136/oem.42.2.101

Němeček, J., Šmilauer, V., Kopecký, L., 2011. Nanoindentation characteristics of alkali-activated aluminosilicate materials. Cem. Concr. Compos. 33, 163–170. https://doi.org/10.1016/j.cemconcomp.2010.10.005

Nikolić, V., Komljenović, M., Marjanović, N., Baščarević, Z., Petrović, R., 2014. Lead immobilization by geopolymers based on mechanically activated fly ash. Ceram. Int. 40, 8479–8488. https://doi.org/10.1016/j.ceramint.2014.01.059

Ostiguy, G., Vaillancourt, C., Begin, R., 1995. Respiratory health of workers exposed to metal dusts and foundry fumes in a copper refinery. Occup. Environ. Med. 52, 204–210. https://doi.org/10.1136/oem.52.3.204

Pacheco-Torgal, F., Castro-Gomes, J., Jalali, S., 2008. Alkali-activated binders: A review. Part 2. About materials and binders manufacture. Constr. Build. Mater. 22, 1315–1322. https://doi.org/10.1016/j.conbuildmat.2007.03.019

Palomo, A., Fernández-Jiménez, A., 2011. Alkaline Activation, Procedure for Transforming Fly Ash into New Materials, Part I: Applications 14.

Palomo, A., Grutzeck, M.W., Blanco, M.T., 1999. Alkali-activated fly ashes A cement for the future. Cem. Concr. Res. 7.

Pan, Z., Cheng, L., Lu, Y., Yang, N., 2002. Hydration products of alkali-activated slag–red mud cementitious material. Cem. Concr. Res. 32, 357–362. https://doi.org/10.1016/S0008-8846(01)00683-4

Provis, J., 2013. Alkali activated materials: state-of-the-art report, RILEM TC 224-AAM. Springer, New York.

Provis, J.L., 2018. Alkali-activated materials. Cem. Concr. Res. 114, 40–48. https://doi.org/10.1016/j.cemconres.2017.02.009

Provis, J.L., 2014. Geopolymers and other alkali activated materials: why, how, and what? Mater. Struct. 47, 11–25. https://doi.org/10.1617/s11527-013-0211-5

Provis, J.L., Bernal, S.A., 2014. Geopolymers and Related Alkali-Activated Materials. Annu. Rev. Mater. Res. 44, 299–327. https://doi.org/10.1146/annurev-matsci-070813-113515

Puertas, F., Ferna, A., 2003. Mineralogical and microstructural characterisation of alkali-activated fly ash/slag pastes 6.

Puertas, F., MartÂõnez-RamÂõrez, S., Alonso, S., VaÂzquez, T., 2000. Alkali-activated fly ash/slag cement Strength behaviour and hydration products. Cem. Concr. Res. 8.

Qian, G., Sun, D.D., Tay, J.H., 2003. Immobilization of mercury and zinc in an alkali-activated slag matrix. J. Hazard. Mater. 101, 65–77. https://doi.org/10.1016/S0304-3894(03)00143-2

Shi, C., Fernández-Jiménez, A., 2006. Stabilization/solidification of hazardous and radioactive wastes with alkali-activated cements. J. Hazard. Mater. 137, 1656–1663. https://doi.org/10.1016/j.jhazmat.2006.05.008

Shi, C., Qian, J., 2000. High performance cementing materials from industrial slags — a review. Resour. Conserv. Recycl. 29, 195–207. https://doi.org/10.1016/S0921-3449(99)00060-9

Škvára, F., Kopecký, L., Šmilauer, V., Bittnar, Z., 2009. Material and structural characterization of alkali activated low-calcium brown coal fly ash. J. Hazard. Mater. 168, 711–720. https://doi.org/10.1016/j.jhazmat.2009.02.089

Tossavainen, A., 1976. Metal fumes in foundries. Scand. J. Work. Environ. Health 2, 42–49. https://doi.org/10.5271/sjweh.2833

van Deventer, J.S.J., Provis, J.L., Duxson, P., Brice, D.G., 2010. Chemical Research and Climate Change as Drivers in the Commercial Adoption of Alkali Activated Materials. Waste Biomass Valorization 1, 145–155. https://doi.org/10.1007/s12649-010-9015-9

Yunsheng, Z., Wei, S., Qianli, C., Lin, C., 2007. Synthesis and heavy metal immobilization behaviors of slag based geopolymer. J. Hazard. Mater. 143, 206–213. https://doi.org/10.1016/j.jhazmat.2006.09.033

Zhang, J., Provis, J.L., Feng, D., van Deventer, J.S.J., 2008. Geopolymers for immobilization of Cr6+, Cd2+, and Pb2+. J. Hazard. Mater. 157, 587–598. https://doi.org/10.1016/j.jhazmat.2008.01.053